Interpretation of the paleo-primary production record in the NW African coastal upwelling system as potentially biased by sea level change

Xavier Giraud, Andre Paul

Interpretation of the paleo–primary production record in the NW African coastal upwelling system as potentially biased by sea level change

Xavier Giraud[1,2] and André Paul[1]

Received 13 May 2009; revised 27 July 2010; accepted 24 August 2010; published 11 December 2010.

[1] Using a regional circulation-ecosystem model subject to a set of boundary conditions that reflect present-day (PD) and Last Glacial Maximum (LGM) conditions, we investigate how changes in preformed subsurface nutrient concentrations as opposed to a local drop in sea level or increase in wind stress influence the biological productivity off the northwest African coastal upwelling area. A reduction of subsurface nutrient concentration at LGM reduced the zonally averaged primary production (PP). The sea level change modifies the shelf morphology, the upwelling circulation, and the productivity and displaces the high-productivity zone. According to our model results, the sedimentary record of PP is best explained by a simulation considering a doubled wind stress over NW Africa. We conclude that production regionally along the coast of NW Africa during the LGM may have been lower than today, despite the fact that most of the sediment cores north of 22°N show local increases in PP during the last glacial period. This paradox may be due to the sea level change and the associated eastward shift of the coastline and upwelling system.

Citation: Giraud, X., and A. Paul (2010), Interpretation of the paleo–primary production record in the NW African coastal upwelling system as potentially biased by sea level change, *Paleoceanography*, *25*, PA4224, doi:10.1029/2009PA001795.

1. Introduction

[2] The major coastal upwelling systems are particularly useful study areas for paleoreconstructions of climate, since they combine the advantage of being highly productive areas, having high sedimentation rates (both from terrestrial and marine components), and being under the influence of changing oceanographic and atmospheric forcing. The primary production (PP) of a coastal upwelling area depends on many factors, including the nutrient load of subsurface waters, the intensity of the upward flux of nutrients, the continental shelf morphology, and the intensity and orientation of the surface wind field. Therefore, reconstructing the PP of regional upwelling systems for past periods goes together with reconstructing climatic and oceanographic fields at larger scale, like the atmospheric wind system or the oceanic nutrient content.

[3] Numerous studies have tried to reconstruct the paleo-productivity and organic carbon fluxes in the NW African coastal upwelling system during Last Glacial Maximum (LGM) and to compare to present-day (PD) conditions. Sedimentary core data from the NW African upwelling area, for which estimates were available for both time periods PD and LGM, are presented in Table 1. These PP data are also presented as relative differences (expressed as "LGM/PD minus 1") and are plotted on Figure 1 (circles). We also plotted the estimates of organic carbon fluxes to the sediments in the Canary region based on benthic foraminiferal faunas by *Eberwein and Mackensen* [2008] (squares in Figure 1).

[4] The general pattern shown by the data is an apparent increase in paleoproductivity during glacial time [*Eberwein and Mackensen*, 2008; *Freudenthal et al.*, 2002; *Hartmann et al.*, 1976; *Sicre et al.*, 2000], except for cores located at the latitude of Cape Blanc (~21°N), where the records show a decreased organic carbon flux [*Martinez et al.*, 1999; *Zhao et al.*, 2000]. In the case of Cape Blanc, *Martinez et al.* [1999] and *Zhao et al.* [2000] conclude that the lower PP is associated with increased wind strength. Therefore, they suggest that the observed decrease in PP may result from changes in direction of the wind system and/or shifts in the position and geometry of the upwelling cell.

[5] The sea level change has been put forth as a possible explanation of variations in ocean fertility off Cape Blanc [*Diester-Haas*, 1983] or in the Canary Islands area [*Freudenthal et al.*, 2002]. During the LGM, the sea level was about 120 m lower compared to the present [e.g., *Bard et al.*, 1996; *Peltier*, 2004], while the continental shelf break at present is located between 100 and 200 m depth in the NW African region. Because of the sea level change, the coastline position can be moved by many tens of kilometers, and the most productive location of the upwelling system, its proximal area, is therefore also shifted. This may change the position of core sites relative to the highly productive upwelling area. Interpreting the variations of organic matter fluxes without considering the changes in relative position of the core site

[1]MARUM – Center for Marine Environmental Sciences and Faculty of Geosciences, University of Bremen, Bremen, Germany.
[2]Now at CEREGE, Aix-Marseille Université, Collège de France, IRD, Europôle de l'Arbois, CNRS, Aix-en-Provence, France.

0883-8305/10/2009PA001795

Table 1. Sediment Core Data and Model Comparison[a]

Reference	Core Site	Location		Depth (m)	Data					Model PP Relative Difference			
					PD Age (kyr)	PD TOC AR ($mg/cm^2/kyr$)	LGM Age (kyr)	LGM TOC AR ($mg/cm^2/kyr$)	TOC AR Relative Diff. (No Dim.)	Std_Geo (Figure 10a)	Dbl_Geo (Figure 10b)	Std_Zonal (Figure 10c)	Dbl_Zonal (Figure 10d)
1	GIK12310–3	23.49°N	18.72°W	3076	0–11	4	11–73	21	4.25	*0*	*0.28*	**–0.58**	**–0.53**
1	GIK12327–5	23.13°N	17.73°W	2046	0–11	44	11–73	390	7.86	*0.038*	*0.13*	**–0.51**	**–0.40**
1	GIK12392–1	25.17°N	16.84°W	2575	0–11	10	11–73	88	7.8	*–0.25*	*0.79*	**–0.82**	**–0.68**
2	ODP 658	20.75°N	18.58°W	2270	4.1	307	19.6[a]	153[b]	–0.5	*–0.024*	**0.40**	**–0.53**	**–0.42**
3	GeoB 4223	29.02°N	12.47°W	775	1	38	18–20	107	1.8	*–0.028*	**1.01**	**–0.62**	**–0.26**
4	GeoB 4240	28.89°N	13.23°W	1358	2.5	15.6	18–20	106	5.8	**–0.29**	**0.87**	**–0.67**	**–0.28**
5	GeoB 4228	29.48°N	12.99°W	1638	0.5–2	22.1	18–20	36.3	0.64	**–0.20**	*0.14*	**–0.34**	**0.44**
6	GeoB 4216	30.63°N	12.4°W	2324	2	8.3	18–20	33.6	3.05	**–0.38**	**–0.27**	**–0.42**	**0.14**
7	SU94–11K	21°N	18°W	1200	2–5	220	18–19	30	–0.86	*–0.02*	**0.65**	**–0.49**	**–0.37**

[a]References: 1, *Hartmann et al.* [1976]; 2, *Tiedemann* [1991]; 3, *Freudenthal et al.* [2001b]; 4, *Freudenthal et al.* [2001c]; 5, *Freudenthal and Kuhlmann* [2001]; 6, *Freudenthal et al.* [2001a]; 7, *Sicre et al.* [2001]. TOC AR, total organic content accumulation rate. Relative differences are computed as (LGM/PD-1). In the "Model PP Relative Difference" columns, values in bold indicate differences in the modeled PP that are statistically significant (Student's t test, $\alpha = 0.05$).
[b]Note that the TOC AR at 20.4 kyr and 21.3 kyr also show high values of 299 and 237 $mg/cm^2/kyr$, respectively (see also the data of *Tiedemann* [1991]).

and the coastline may lead to biased estimations of the upwelling productivity.

[6] The decreased PP inferred off Cape Blanc may also result from a lower nutrient concentration of the Atlantic central waters, as indicated by nutrient proxy data [*Eberwein and Mackensen*, 2008; *Rühlemann et al.*, 1999; *Sigman et al.*, 2003]. However, the reduced subsurface nutrient concentration should also have induced a reduction of the PP in the more northern part of the NW African upwelling, which is not what seems to be indicated by the sedimentary data mentioned above.

[7] Other physical processes are potentially responsible for changes in the record of the PP, including advection or sediment transport processes, and finally potential diagenetic transformations. Potential post-depositional transformation of the primary signal can be estimated by chemical proxies, e.g., authigenic minerals occurrence, degree of preservation of foraminiferal tests and stable isotope composition [e.g., *Freudenthal et al.*, 2001]. The impact of lateral advection in the water column or sediment remobilization and transport are difficult factors to estimate. Belts of sediment accumulation like the slope depocenter off Cape Blanc between 1000 and 2000 m depth are partly known [*Fütterer*, 1983]. Nevertheless, it is sometime possible to evaluate the focusing and winnowing of sediments [e.g., *François et al.*, 2004; *Mollenhauer et al.*, 2007]. Because of the difficulty to estimate all the sediment and organic matter transport processes, most of paleoproxy studies follow two interpretation pathways. First, the organic matter accumulation and other proxy measurements can be considered as representative of the situation above the core location only, neglecting any lateral component. This may be true if the core is located far

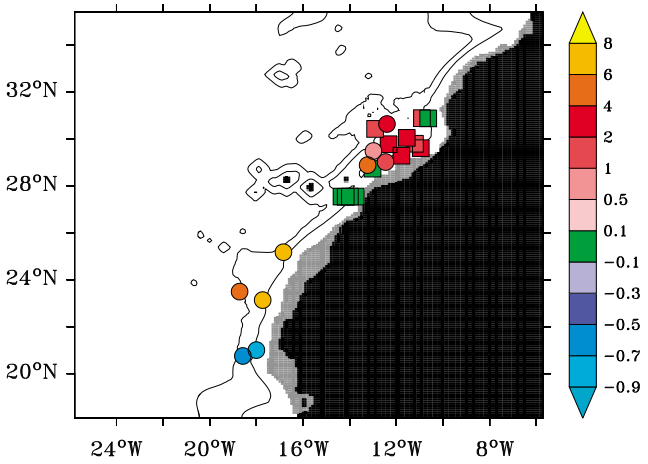

Figure 1. Relative difference of PP between LGM and PD (LGM/PD-1) as reported in Table 1 (circles). Squares are data from *Eberwein and Mackensen* [2008, Table 6], who estimated the organic carbon fluxes at PD and LGM as very low, low, intermediate, or high. We therefore plotted a relative difference of 0, 1, or 2, if the organic carbon fluxes between PD and LGM were at the same intensity (green squares), if the LGM flux estimations were one level higher than the PD fluxes, or if LGM flux estimations were two levels or more higher than the PD fluxes, respectively.

enough from the coast. Alternatively, the organic matter accumulated on the continental slope can originate from a wider area, the surface production signal between the coast and the core location being mixed and altered by transport mechanisms. In this case, results and conclusions from a particular location can be extended to the whole upstream upwelling system, implicitly assuming accumulation and mixing processes of the surface production signal. Both approaches can be correct, but should be considered carefully and do not necessarily have the same implications. The origin of the sediments is therefore a major aspect in the interpretation of the sedimentary records.

[8] This study aims to investigate the impact of sea level change on surface PP distribution by using a three-dimensional modeling approach with relatively high resolution (~10 km). This resolution allows for a relatively detailed representation of the continental shelf and therefore of changes in bathymetry induced by a sea level change. By comparing one PD and three LGM simulations, we have tried to identify how important can be the sea level effect on the variations of the sedimentary signal over the continental slope. We have also tried to evaluate the relative contribution of the different driving processes (subsurface nutrient concentration, wind stress and upwelling geometry) to the variations of PP.

2. Model Description

2.1. Ocean Circulation Model: ROMS

[9] The oceanic circulation is simulated by the Regional Ocean Modeling System (ROMS), which solves the primitive equations based on the incompressible and hydrostatic approximations, with a free sea surface, horizontal curvilinear coordinates, and a generalized terrain-following vertical grid. A complete description is given by *Shchepetkin and McWilliams* [2003, 2005]. The grid is set with 20 vertical levels, with surface and bottom refinement using the stretching parameters $\Theta_s = 5.0$ and $\Theta_b = 0.4$, to allow for a better representation of the surface and bottom boundary layers. The topography is obtained by linear interpolation of the ETOPO5 data [*National Geophysical Data Center*, 1988]. Depths shallower than 20 m are reset to 20 m, and the topography is smoothed with a maximum slope parameter ($r = grad(h)/h$, where h is depth) of 0.2. The vertical mixing coefficients for momentum and tracers in the ocean interior are calculated according to the non-local K-Profile Parameterization (KPP) scheme by *Large et al.* [1994]. In particular, we used version 1.1 of ROMS-AGRIF [*Penven et al.*, 2006]. Taking advantage of the AGRIF (Adaptive Grid Refinement in Fortran) package [*Blayo and Debreu*, 1999; *Debreu*, 2000; *Debreu et al.*, 2008], it is possible to design an embedded grid with a higher resolution focused on a regional area. We use therefore a nesting approach in order to set up a high-resolution model of the NW African margin, and an intermediate-resolution model of the Atlantic Ocean. The high-resolution grid, the "child" grid, is centered on our study area, between 18.05°N–35.5°N and 25.8°W–5.7°W, while the intermediate-resolution grid, the "parent" grid, extends over the entire width of the Atlantic Ocean from 25°S to 43.5°N. The scale factor between the two embedded grids is set to 5, so that the parent and the child grids have resolutions of 1/2° and 1/10°, respectively, and baroclinic time steps of 5760 s and 1152 s, respectively. The number of barotropic time steps between baroclinic time steps is set to 45.

2.2. Biogeochemistry Model: NPZD

[10] We used an NPZD (Nutrient, Phytoplankton, Zooplankton and Detritus) biogeochemical model, as described by *Oschlies and Garçon* [1999] and already used by *Giraud et al.* [2000, 2003] in the context of the Mauritanian upwelling region. The only change compared to the model description by *Oschlies and Garçon* [1999] is the implementation of a varying sinking rate of the detritus, as already introduced by *Giraud* [2006]. This varying sinking rate is motivated by the fact that some studies suggest that the vertical sinking velocities are low in the mixed layer and increase with depth, due to aggregation processes [*Berelson*, 2002; *Klaas and Archer*, 2002; *Kriest*, 2002; *Kriest and Evans*, 1999]. The sinking rate of detritus is therefore 5 m d^{-1} in the upper 50 m and then increases exponentially with a scale-height of 200 m and a maximum sinking rate of 200 m d^{-1} [see also *Giraud*, 2006, equation (15)].

[11] The transport of the biogeochemical state variables by the oceanic circulation is implicitly taken into account by the advection scheme of ROMS. No resuspension of detritus at the bottom is considered. Detritus reaching the seafloor is instantaneously remineralized and added to the nutrient pool in order to avoid a loss of mass. It is therefore not possible to comment on a realistic distribution of the detrital sediments in the model. However, uncertainties on sediment transport processes are still large in modeling studies, partly because of the difficulty to appropriately represent the remineralization terms during the transport itself. Therefore, our study focuses on the intensity and spatial distribution of PP in the surface ocean. The potential impact of processes of transport and settling to the sediments is part of the discussion and interpretation.

3. Description of Simulations

[12] Four different regional simulations using the ROMS/NPZD model were performed (Table 2). They differ from each other only in their initial and boundary conditions. The surface boundary conditions, as well as the (physical and biogeochemical) initial conditions and lateral boundary conditions for the coupled regional circulation-ecosystem model (ROMS/NPZD), were provided by global simulations performed with the University of Victoria Earth System-Climate Model (UVic ESCM) version 2.8 [*Weaver et al.*, 2001]. This model includes the Modular Ocean Model (MOM) version 2 [*Pacanowski*, 1995], a thermodynamic-dynamic sea-ice model and a vertically integrated atmospheric energy-moisture balance model. The horizontal resolution is coarse (3.6° in longitude and 1.8° in latitude), with 19 vertical levels in the ocean. The UVic ESCM also contains a description of the terrestrial vegetation and carbon cycle [*Meissner et al.*, 2003], as well as of the marine biogeochemistry and ecosystem [*Schmittner et al.*, 2008]. The UVic ESCM is driven by seasonal and latitudinal variations

Table 2. Descriptions of Simulations[a]

Simulation	Orbital and pCO2atm Configuration/Wind Stress Forcing	NADW Formation (Sv)	NADW Export (Sv)	Max. Transport of North Atlantic Subtropical Gyre (Sv)	Subsurface NO_3 in the Child Domain (mmol N m^{-3})
PD	Present day/NCEP/NCAR wind stress	18	12	45	16.1
LGMpd	LGM/NCEP/NCAR wind stress	12	8	35	7.4
LGMstd	LGM/CCSM3 wind stress anomaly added	16	12	51	10.9
LGMdbl	LGM/CCSM3 wind stress anomaly added Plus doubling over NW African coast only in ROMS[b]	16	12	51	11.5

[a]See text in section 3.
[b]See Appendix A.

in solar radiation incident at the top of the atmosphere. The surface wind stress to force the ocean and the winds for the advection of heat and moisture in the atmosphere must be prescribed from a monthly climatology. The extent and height of the continental ice sheets are prescribed according to *Peltier* [2004]. The full description and interpretation of the global UVic ESCM simulations are given by *Kageyama et al.* [2010].

[13] Each global experiment performed with the UVic ESCM has been run until a near-equilibrium in the circulation was reached (i.e., a few thousand of years). Each associated ROMS/NPZD regional simulation starts with the near-equilibrium state provided by the UVic ESCM simulation, and is performed over a total duration of 30 years. During the first 16 years, the oceanic circulation only is computed, applied on the parent grid only (Atlantic domain of 1/2° resolution). During the next 8 years, the biogeochemistry and the physics are coupled and applied on the parent grid only. The first 24 years constitute therefore the spin-up phase. Its goal is to ensure the transition from the initial conditions from the coarse resolution global model to the new equilibrium of the finer resolution regional model. After this spin-up phase, the coupled model is applied on both parent and embedded-child grid (NW African domain of 1/10° resolution) for another 6 years. The results of these last 6 years only, within the high-resolution domain, are used for interpretation.

[14] Simulation PD is set up for a present-day configuration. For the global UVic ESCM control experiment, Earth's orbital parameters [*Berger*, 1978] were set to their AD 1950 values, the atmospheric CO_2 concentration was set to 280 ppmv, the present-day configuration of the continental ice sheets was used and the monthly wind stress and wind fields were taken from the NCEP reanalysis climatology [*Kalnay et al.*, 1996].

[15] Simulation LGMstd is set up for a standard LGM configuration. For the global UVic ESCM setup, Earth's orbital parameters were set to values appropriate for 21,000 years before present, the atmospheric CO_2 concentration was set to 200 ppmv and the LGM configuration of the continental ice sheets was used. The monthly wind fields were also taken from the NCEP reanalysis climatology, but the monthly wind stress fields were obtained by adding the wind stress anomaly from a coupled atmosphere-ocean general circulation model (NCAR CCSM3) [cf. *Otto-Bliesner et al.*, 2007]. Regional features (like stronger winds at coastal regions) are therefore resolved from the NCEP reanalysis, and the CCSM3 wind stress LGM anomaly adds synoptic changes to the wind stress field. The LGM topography is obtained by simply subtracting 120 m to the original ETOPO5 data [*National Geophysical Data Center*, 1988] before interpolation.

[16] Simulation LGMpd has mixed forcing conditions and is set for sensitivity analysis only. The orbital parameters and atmospheric CO_2 concentration were similar to the LGMstd simulation, but it uses the present-day NCEP/NCAR reanalysis surface wind stress [*Kalnay et al.*, 1996].

[17] Simulation LGMdbl has the same settings and boundary conditions as simulation LGMstd, but with an intensified (doubled) wind stress localized over the NW African coast (see Appendix A for a description of the modification applied to the wind stress field). This sensitivity experiment is motivated by studies based on dust and terrestrial biomarkers analyses which suggest a strengthening of major wind patterns over NW Africa [e.g., *Martinez et al.*, 1999; *Parkin*, 1974; *Parkin and Shackleton*, 1973; *Sarnthein et al.*, 1981; *Sicre et al.*, 2000, 2001; *Zhao et al.*, 2000]. The increased wind stress has been applied to the regional ROMS simulation only, not to the global UVic ESCM simulation. The UVic LGM settings (orbital parameters, atmospheric CO2 concentration and continental ice sheet) and wind stress (CCSM3 anomaly added) are therefore identical between LGMstd and LGMdbl.

4. Results

4.1. Evaluation of the Model

4.1.1. Basin Scale Circulation

[18] The main differences between the LGM and PD simulations with the global climate model are the generally colder climate and the reduced ventilation of the deep ocean. When PD wind and wind stress fields but otherwise glacial boundary conditions were used (simulation LGMpd), the formation of North Atlantic Deep Water (NADW) and its export to the South Atlantic Ocean were reduced by 30%, and the transport of the Gulf Stream, along with the strength of the North Atlantic subtropical gyre, weakened by 20%, as compared to simulation PD (Table 2). When the monthly wind stress fields were modified with the anomaly from the NCAR CCSM3 model (simulation LGMstd), the North Atlantic subtropical gyre strengthened by 15%; consequently, the NADW formation was only slightly reduced

(by 10%) and the NADW export was even comparable to simulation PD.

[19] The average nutrient concentration of the thermocline or central waters (between 150 and 800 m depth) in the child domain (i.e., in the focused study area) is about 16.1 mmol N m^{-3} in simulation PD (Table 2), which is comparable to the observed World Ocean Atlas value of 16.8 mmol N m^{-3} [*Garcia et al.*, 2006]. This comparison shows a better agreement than the global UVic ESCM results before the ROMS spin-up phase of 24 years. The higher resolution and different mixing scheme of the ROMS model compared to the coarse resolution UVic model helps to improve the modeled thermocline ventilation just south of our study area.

[20] Our LGM simulations showed a nutrient depletion of this thermocline or central waters of about 32%, with average concentrations of 16.1 and 10.9 mmol N m^{-3} for the PD and LGMstd, respectively (Table 2). This seems to be in agreement with paleonutrient reconstructions based on proxy data (e.g., $^{13}C/^{12}C$ or Cd/Ca ratio of benthic foraminifera tests) indicating lower nutrient concentrations of Atlantic central waters [*Eberwein and Mackensen*, 2008; *Sigman et al.*, 2003, and references therein]. *Rühlemann et al.* [1999, and references therein] also concluded that glacial intermediate waters were depleted in nutrients.

4.1.2. Regional Circulation and Biogeochemistry

[21] The model results of the high-resolution grid reproduced a realistic picture of the present-day annual-mean Sea Surface Temperature (SST, Figure 2a), as compared to data (Figure 2g) [*Armstrong and Vazquez-Cuervo*, 2001]. The coldest SSTs along the coast were in agreement with observations, both for the annual mean or seasonal values. Minimum modeled annual mean SST was 16.2°C.

[22] The upwelling index, defined as the temperature anomaly between the coastal and offshore SSTs, also showed a realistic seasonality (Figure 3a). From November to May, the maximum SST anomaly occurred at the latitude of Cape Blanc, between 20°N and 24°N, while more northern latitudes showed a positive upwelling index. In summer, the upwelling index showed strong negative values at around 30°N, indicating the strong upwelling activity, while it became slightly positive south of Cape Blanc. This corresponds to the seasonality of the upwelling index as described by *Speth and Detlefsen* [1982]. The proper modeling of the coastal SSTs associated to the onshore offshore SST gradient and its seasonality indicate that the model captures the upwelling dynamics realistically at this regional scale.

[23] The surface chlorophyll-a (Chl-a) concentration is not a state variable of the model, but can be estimated using a constant Chl-a/N ratio of 1.59 mg Chl-a (mmol N)$^{-1}$ [*Oschlies and Garçon*, 1999] applied to the surface phytoplankton concentration. Maximum values for modern in situ measurements of chlorophyll-a concentrations in the Mauritanian upwelling are up to 3.5 mg Chl-a m^{-3} [*Fischer et al.*, 1996; *Gabric et al.*, 1993; *Morel*, 2000], while SeaWiFS remote data indicate much higher values close to the coast (Figure 4). These high values may be overestimated because of the presence of gelbstoff and various types of suspended particles in coastal environments. The model does not simulate such high values along the coast, that may or may not be Chl-a, but does simulate the proper extent of the annual mean surface Chl-a concentration in the Mauritanian upwelling (Figure 4), with a maximum value of about 2.0 mg Chl-a m^{-3}. At the EUMELI eutrophic site off Cape Blanc, the annual mean PP reached a maximum of 421 gC m^{-2} yr^{-1} (Figure 5a), slightly lower than the value mentioned by *Morel* [2000] of about 535 gC m^{-2} yr^{-1}.

4.2. How to Compare PD and LGM Records?

[24] The conditions prevailing in producing a sedimentary record have obviously changed in time. Among these, the transport (lateral advection or bottom-sediment remobilization) is of prime importance. The following is an attempt to over-simplify the complex problem of sediment transport and distribution, and to draw general lines to help the interpretation of the model results, considering that the sediment transport is not explicitly modeled.

[25] According to *Fütterer* [1983], the sediment distribution over the continental shelf off Cape Blanc is mainly made of coarse-grained carbonate sand derived primarily from mollusk and plankton shell debris. *Fütterer* [1983] interprets this distribution as the effect of the action of the Canary Current, which is at present strong and deep enough to winnow fine material from the shelf and upper continental slope, and even partly to erode the continental shelf. A large fraction of the shelf sediments is therefore transported downslope in suspension by a nepheloid layer or grain-by-grain. As a consequence, organic matter accumulates off Cape Blanc between 1000 and 2000 m depth in a slope depocenter.

[26] We can therefore distinguish between two extreme situations: some locations are strongly influenced by the lateral advection and sediment transport and therefore record what we call a zonally cumulative signal, while some other locations are not or poorly influenced by the lateral mixing processes, and therefore record what we call a local signal. The former may be located nearer the shore or in upper-slope positions and the latter are offshore or lower-slope positions. The comparison of the variations between PD and LGM at the different locations in the model outputs is therefore also made using two approaches. For the locations not or poorly influenced by the lateral advection, we compute the simple difference of the signal at geographical locations (section 4.3). For the locations strongly influenced by the lateral mixing components, and where the signal is therefore representative of a wide area, we compute and then compare the zonally cumulative signal (section 4.4).

[27] Both at PD and LGM periods, both kinds of behavior of the sedimentary records (influenced or not by the lateral advection) certainly occur on the margin. We can even probably expect that the margin shows a gradient between onshore locations that are highly influenced by lateral advection terms and offshore locations that are moderately or not at all influenced by lateral advection terms. Whether a particular location on the margin experiences different situations (with or without lateral advection influence) between PD and LGM is another important aspect that is more difficult to estimate.

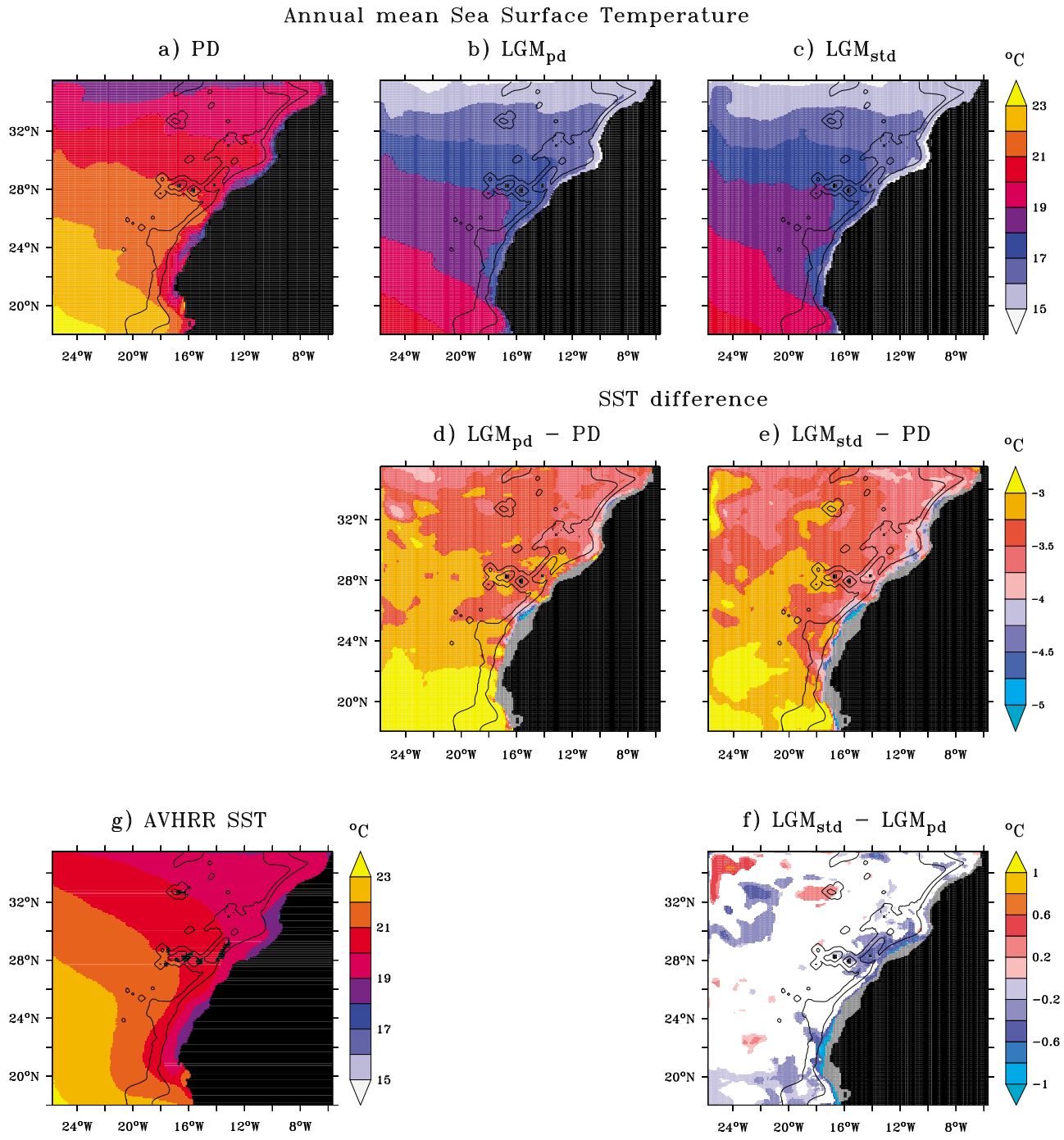

Figure 2. Annual mean SSTs and SST difference (°C). (a) PD, (b) LGMpd, (c) LGMstd, (d) LGMpd-PD, (e) LGMstd-PD, (f) LGMstd-LGMpd, and (g) data from the AVHRR Pathfinder Global 9 km Pentad SST Climatology [*Armstrong and Vazquez-Cuervo*, 2001].

[28] Three areas can be conceptualized, according to their relative position to the PD coastline. In the first case, we would find modern locations that are close to the coast and therefore under the influence of lateral advection. At low sea level stand of the LGM, if they are not on the emerged shelf, they would still be close to the coast and under the influence of lateral mixing processes as well. The comparison of the sedimentary signal at these locations fall under the comparison of zonally cumulative distribution maps of both PD and LGM simulations, as presented in section 4.4. In a second case, we would find locations that are far enough from the coast to be safe from the lateral advection and sediment reworking processes both at PD and at LGM. The comparison of the sedimentary signal at these locations is

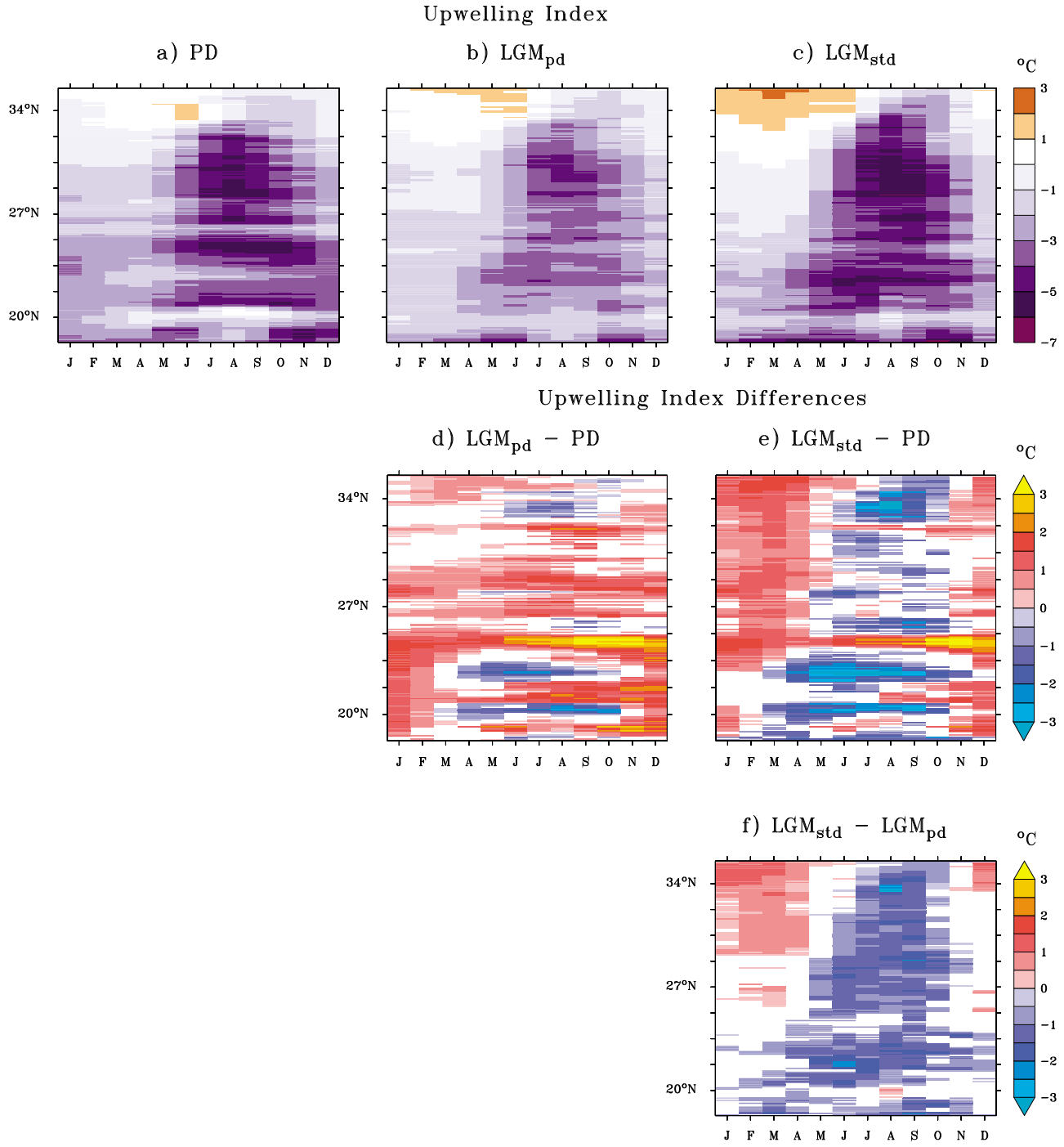

Figure 3. Upwelling index and upwelling index difference (°C). (a) PD, (b) LGMpd, (c) LGMstd, (d) LGMpd-PD, (e) LGMstd-PD and (f) LGMstd-LGMpd. In Figures 3d–3f, white areas indicate results that are statistically not significant (Student's t test, $\alpha = 0.05$). The upwelling index is computed here as the SST difference between a coastal band (the three nearest ocean grid points to the continent) and an offshore band (30 grid points large, distant from the coast by 75 grid points).

done while comparing the records at geographical locations (section 4.3).

[29] The third case would consider locations of intermediate positions. At PD, these locations are not or poorly influenced by the lateral advection or sediment transport processes since they are far enough from the coast. During the low sea level stand of the LGM, the coastline being shifted offshore, the locations become closer to the coast and may then be under the influence of the lateral mixing terms. To be able to make a comparison of these two situations, at

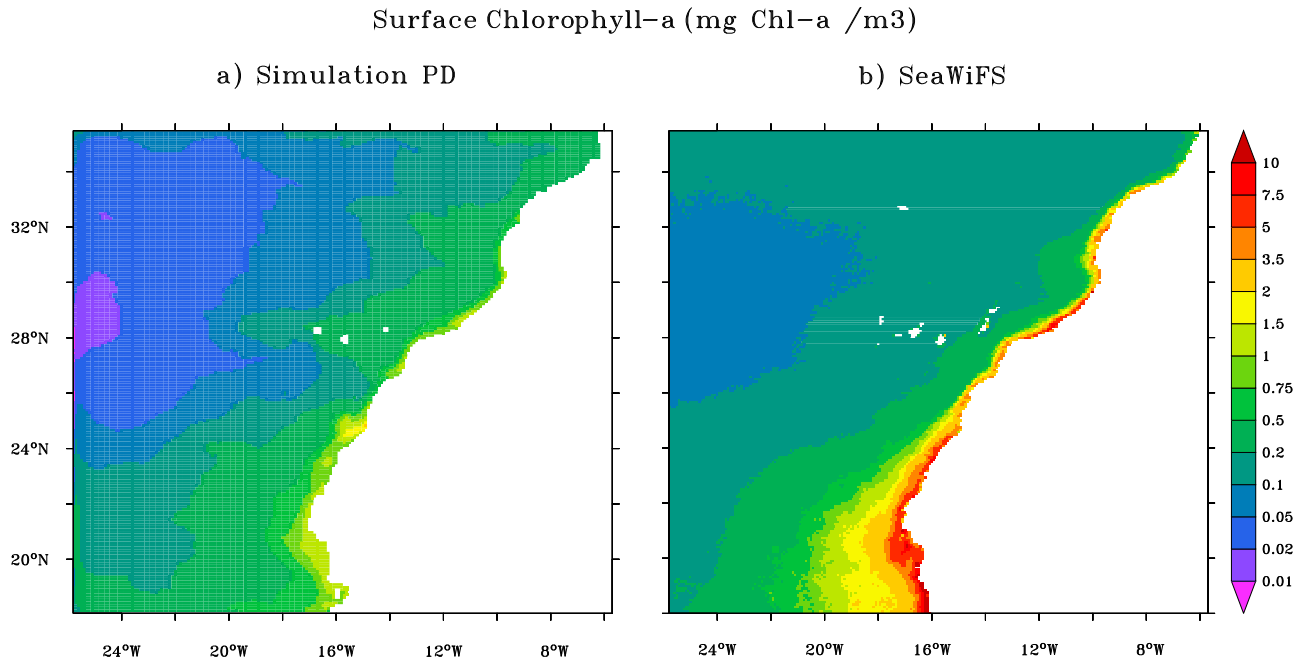

Figure 4. Surface chlorophyll-a concentration (mg Chl-a m^{-3}) (a) for simulation PD and (b) from SeaWiFS data.

PD and LGM, we would need to compare the zonally cumulative production of the LGM simulation, to the local production of the PD simulation. This is unfortunately not possible with our model. The locally produced and the zonally cumulative PP lead to strongly different estimations in the magnitude of the sedimentary record. This is because we do not estimate the loss of organic matter in the sediment remobilization process or in early diagenesis. This is also the reason why we prefer to present relative differences rather than absolute differences, when comparing data and model results in section 5.

4.3. Comparisons at Geographical Location

[30] All regional simulations (PD and LGM) were performed on the same horizontal parent and child grids. The sea level variation induced a change in the coastline location and in the land-sea mask of a few grid points. In the present section, we will compare the results by subtracting one field from another. This is a simple comparison at geographical locations. In this case, the continental shelf that emerged due to sea level change appears gray-shaded on maps. In section 4.4, we will consider the fact that the shift of the coast line is also a shift of the upwelling structure compared to the sedimentation locations on the continental slope. Therefore, we performed additional analyses of various criteria (PP, nutrient fluxes at the bottom of the mixed layer) computed between any fixed geographical location (which can be a core location) and the associated position on the coastline, moving from PD to LGM simulations. The last six years of simulation showed internal inter-annual variability. We could therefore calculate annual means as well as standard deviations of the various parameters. Based on these two terms, we performed Student's t test comparisons to evaluate whether the means of simulations were significantly different or not.

4.3.1. Primary Production

[31] Figure 5 shows the vertically integrated PP of the simulations LGMpd and LGMstd in comparison to the PD simulation, at each geographical location. The PP of both LGM simulations appeared to be lower than or not significantly different from the PD values (Figures 5d and 5e, Student's t test, $\alpha = 0.05$). In the case of simulation LGMstd, most of the locations between isodepths 1000 m and 3000 m (where most of the sedimentary cores are located; see also Table 1), in the latitudinal band between 20°N and 27°N, do not show a significant change in PP. An increase of the PP can only be observed in the upper most part of the continental slope, close to the LGM coastline and in the North West corner of the child domain, which is not related to the upwelling activity. The comparison of the two LGM simulations shows a more productive situation for the LGMstd conditions than for LGMpd (Figure 5f).

[32] This comparison at any given geographical location assumes a direct link between the PP, the export production and the vertical transport of the organic matter from the surface to the bottom, and no impact of lateral advection or bottom sediment remobilization. As mentioned in section 4.2, this assumption may be true only for the most offshore or mid- to lower-slope positions. Following this assumption, these results mean that the LGM sediments of cores located in this area would not record any significant change of PP compared to PD, also usually interpreted as no change in the upwelling activity.

4.3.2. SST

[33] Figure 2 shows the difference of SSTs between the LGMpd, LGMstd and PD simulations. Both LGM simula-

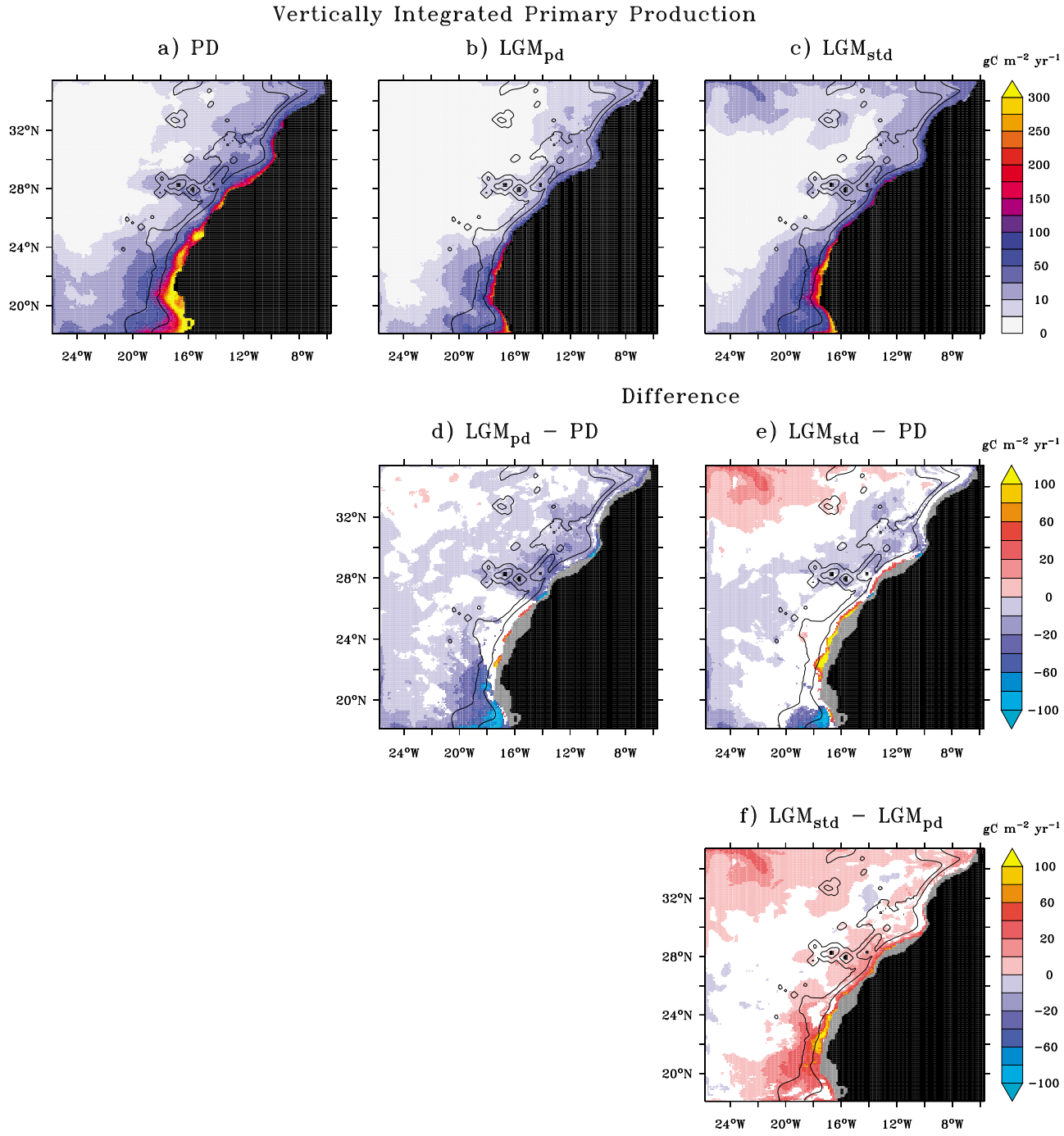

Figure 5. Vertically integrated primary production (gC m^{-2} yr^{-1}). (a) PD, (b) LGMpd, (c) LGMstd, (d) LGMpd-PD, (e) LGMstd-PD, and (f) LGMstd-LGMpd. In Figures 5d–5f, white areas indicate results that are statistically not significant (Student's t test, $\alpha = 0.05$).

tions showed a general cooling of about 3 to 4°C over the NW African domain compared to the PD, with a latitudinal gradient toward slightly stronger SST cooling in the north. This cooling corresponds to a general trend at the large scale of the North East Atlantic Ocean. Stronger SST cooling from 4 to 5°C occurs only in restricted areas along the LGM coastline, i.e., on the uppermost part of the continental slope, at depths shallower than 800 m. It seems therefore that locations on the middle to lower continental slope are not in a position to record a change in the upwelling activity with the temperature proxy, but only the general LGM cooling of the North East Atlantic Ocean.

4.4. Zonal Comparison

4.4.1. Upwelling Index

[34] Figure 3 shows the evolution of the upwelling index for the different simulations. The simulation LGMpd showed less negative values of upwelling index at all latitudes and months, except north and south of Cape Blanc (21°N) and north of Cape Ghir (30°N) in summer, where the upwelling index is more negative. The upwelling seems therefore generally weaker for LGMpd than for PD, except for the summer period of restricted locations as mentioned above.

[35] The simulation LGMstd showed a larger seasonal contrast than the simulation LGMpd, with a weaker upwelling activity (more positive or less negative upwelling index) in winter months at all latitudes, and a stronger upwelling activity (more negative upwelling index) from spring to fall in the southern part of our study area and in summer in the northern part.

[36] This larger seasonal contrast of the upwelling index may explain the fact that annual-mean SST differences (Figure 2e) did not show remarkable cooling that we could relate to a change in the upwelling intensity: colder coastal SSTs in summer may be compensated for by the relatively weaker upwelling in winter. North of 30°N, the upwelling index of LGMstd showed positive values from January to April, indicating that no upwelling occurred. The comparison of LGMstd and LGMpd showed also a strong seasonal contrast. Simulation LGMstd showed a stronger and weaker upwelling activity in summer and winter, respectively.

4.4.2. Zonally Cumulative Primary Productivity

[37] Figure 6 shows maps of zonally cumulative annual mean PP between any given location and the coast. It provides direct information on the total PP produced between the coast and a given point. From the point of view of sedimentation settings, this zonal integration is a first order approximation, which does not consider processes like alongshore advection and sediment transport, or remineralization. For offshore positions far away from the coast, such cumulative production is not relevant, since the location may not be influenced by the coastal production. Figure 6 shows that the annual mean zonal production from the coast to the offshore positions is lower at any location for the LGMpd and LGMstd simulations compared to the PD. Both LGM simulations showed less productive conditions.

[38] The LGMpd results showed a reduced zonally cumulative PP at all latitudes, except for a narrow band at ~27°N, for which differences are statistically not significant (Figure 6d). This result can be related to the general weakening of the upwelling activity as shown by the upwelling index (Figure 3d), and with the apparent decrease of PP at geographical location as observed in Figure 5d. For simulation LGMstd, there is a mismatch between the zonally cumulative PP as shown in Figure 6e and the PP at geographical locations as shown on Figure 5e. The PP at geographical locations mostly showed little variation, while the zonally cumulative PP showed a significant decrease.

4.4.3. Fluxes and Nutrient Concentration at the Mixed Layer Depth

[39] The PP of the surface ocean in coastal upwelling areas is supported by the inflow of the deep nutrients from the sub-surface layer. In order to find out the reasons for the PP variations in the different simulations, we computed and compared this inflow of deep nutrients at a defined bottom boundary. We chose the Mixed Layer Depth (MLD), which has the advantage of defining a surface layer with homogeneous properties (e.g., nutrient consumption) due to the mixing, and seasonal evolution. The MLD is defined here as the depth where the water temperature is 0.8°C lower than the SST [*Kara et al.*, 2000]. When the mixed layer extends to the bottom of the ocean, no vertical flux is computed. The vertical fluxes at MLD are computed and zonally averaged from the coast (or the continental slope if the mixed layer extends to the bottom) to the 3000 m isodepth.

[40] For all simulations, the MLD followed a seasonal cycle, with a deepening in winter and a shoaling in summer (Figures 7a, 7b, and 7c). Simulation LGMpd showed deeper MLD at all latitudes and months compared to simulation PD, except for some locations during summer months that showed no significant change. The maximum deepening was ~60 m in February–March in the northern part (Figure 8d). Simulation LGMstd showed a deeper MLD than simulation PD north of 30°N, with a maximum deepening in February–March, while the southern part showed either a shallowing of the MLD or no change (Figure 7e). The MLD was shallower in simulation LGMstd than in simulation LGMpd in winter at all latitudes, whereas it showed mostly no significant change in summer between the two (Figure 7f).

[41] The vertical velocities at the MLD are shown on Figure 8. Compared to the simulation PD, both LGM results showed a larger seasonal contrast in the vertical velocities at MLD: the summer period showed increased upwelling, while the winter period showed lower values or no change (Figures 8d and 8e). In the annual mean, the signal was too noisy and too close to the statistical significance level to be interpreted as different. There was no significant difference between the results of LGMstd and LGMpd (Figure 8f).

[42] Since simulation LGMpd used the PD wind field, the difference of upwelling intensity between these two simulations was a response to the changes of topography, i.e., the change of orientation of the wind stress compared to the coastline and continental shelf. Without changing the wind field, changing the sea level by 120 m between the PD and LGM by itself affected the seasonality and intensity of the upwelling (upwelling index, MLD, vertical velocities at the MLD).

[43] Considering that the LGMstd and LGMpd configurations have the same topography, the difference of upwelling intensity between these two simulations is a response to the local wind stress only. Therefore, the result of Figure 8f implies that in a low sea level configuration, the change of the wind field from LGMpd to LGMstd may not affect significantly the upwelling intensity.

[44] The concentration of nutrients at the MLD showed a similar seasonal variability for all simulations, with higher concentrations in winter months (Figures 9a, 9b, and 9c). This seasonal cycle partly followed the deepening of the MLD already observed in Figure 7. The winter deepening of the MLD led to an input of deep nutrients to the mixed layer and sustained a winter PP (not shown).

[45] Both LGM simulations showed a general decrease of the nutrient concentration at MLD compared to the PD

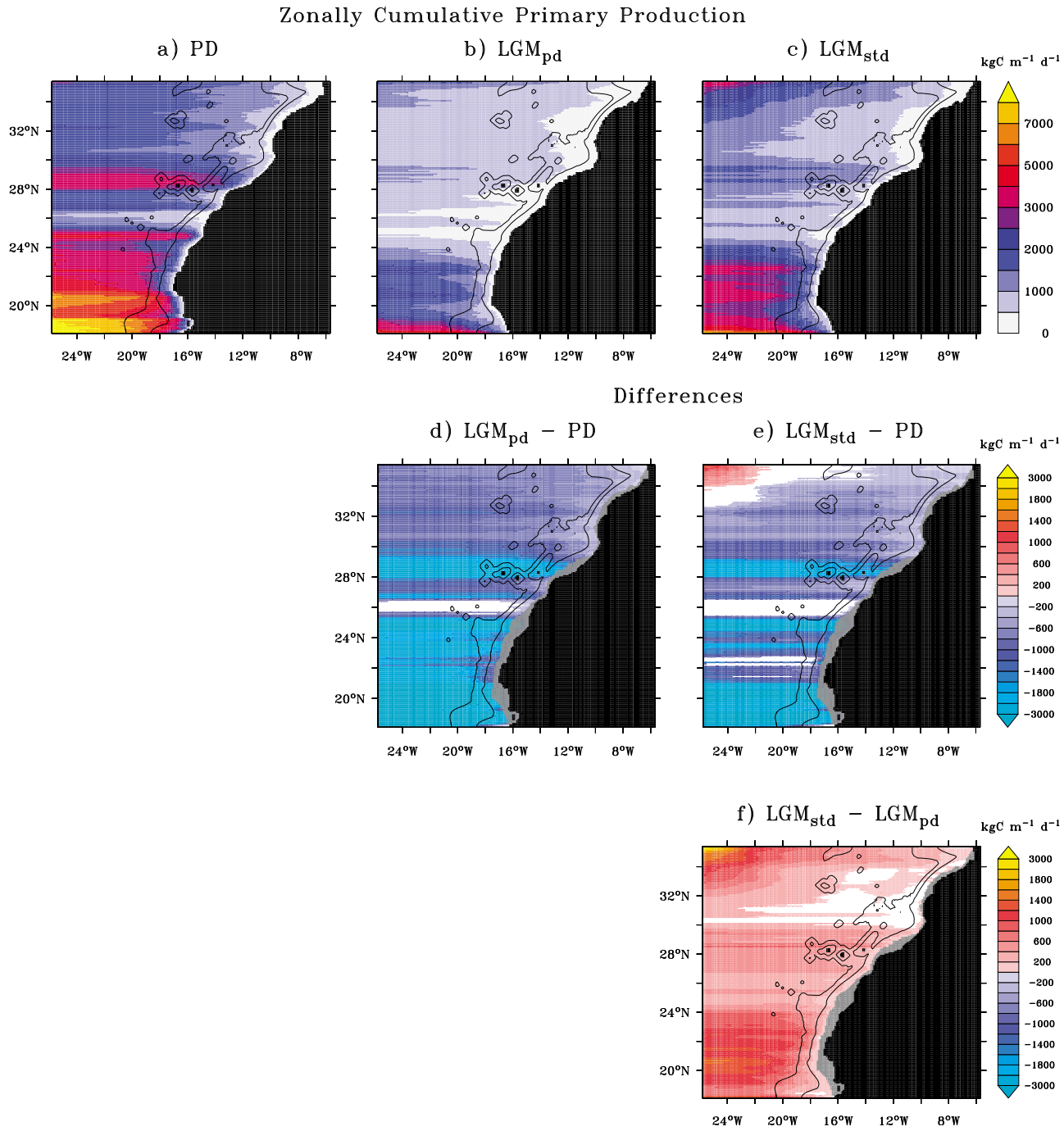

Figure 6. Annual mean of the zonally cumulative PP between any location and the coast (kgC m^{-1} d^{-1}). (a) PD, (b) LGMpd, (c) LGMstd, (d) LGMpd-PD, (e) LGMstd-PD, and (f) LGMstd-LGMpd. In Figures 6d–6f, white areas indicate results that are statistically not significant (Student's t test, $\alpha = 0.05$).

simulation, with a maximum decrease south of 21°N all year long, and in winter periods at all latitudes. For simulation LGMstd, a large band between 22°N and 26°N did not show any significant change compared to PD. North of 26°N, the summer period did not show significant changes, whereas the winter period showed a decrease in nutrient content at MLD. The LGMstd showed higher nutrient concentrations than LGMpd in winter at all latitudes and in summer north of 26°N.

5. Discussion

5.1. Model-Data Comparison

[46] The comparison of the data and model results as presented in Figure 10 highlights two major issues. First, the

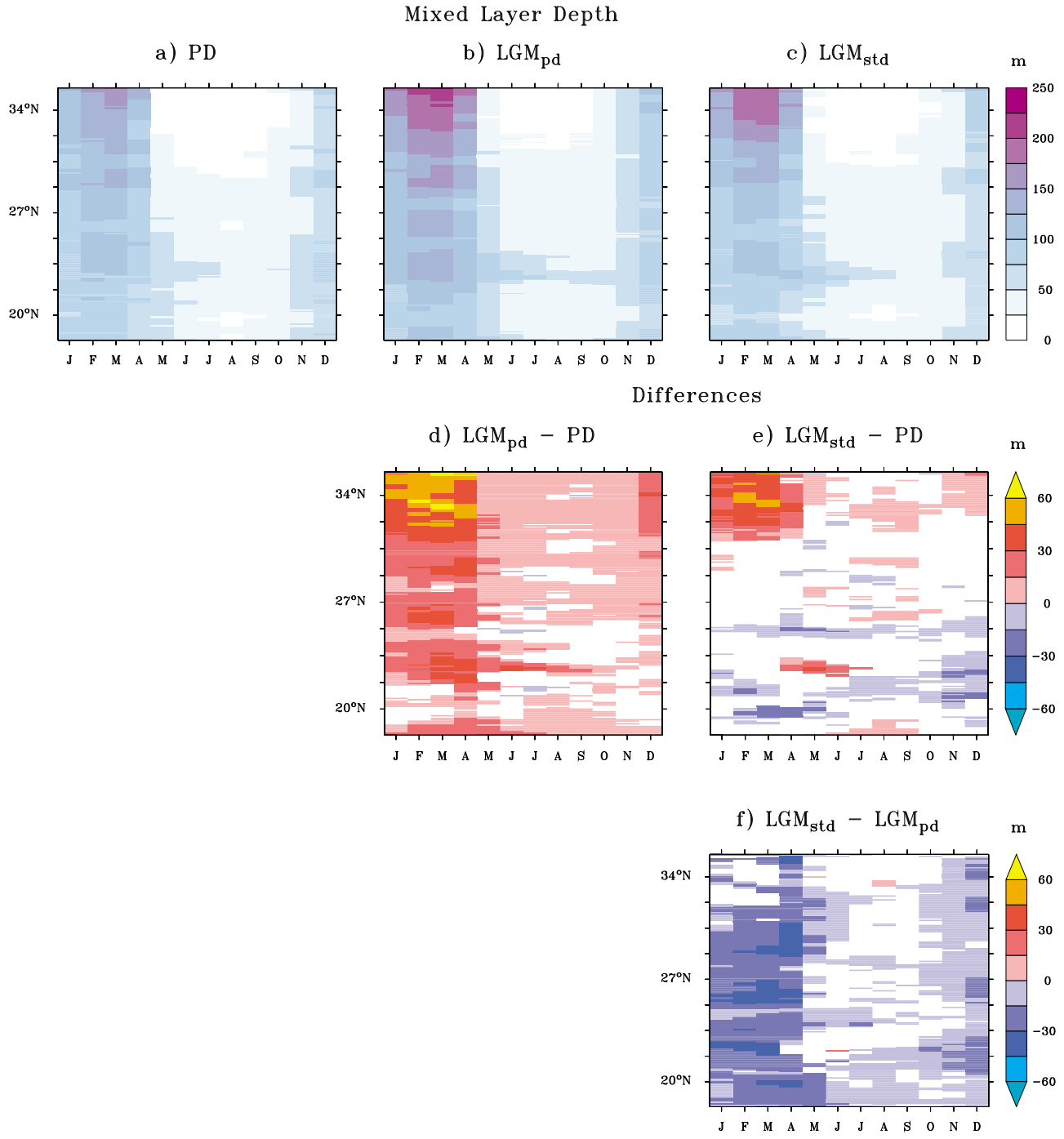

Figure 7. MLD (m) averaged from the coast to the isodepth 3000 m. (a) PD, (b) LGMpd, (c) LGMstd, (d) LGMpd-PD, (e) LGMstd-PD, and (f) LGMstd-LGMpd. In Figures 7d–7f, white areas indicate results that are statistically not significant (Student's t test, $\alpha = 0.05$).

two approaches of interpreting the model results (local versus zonally cumulative record of the PP, Figure 10a versus Figure 10c) disagree with each other. Second, none of the two approaches match to the data when considering simulation LGMstd.

[47] First, the fact that the two approaches of interpreting the model results disagree with each other highlights that the LGM to PD trend of the PP at a given core location can be different from the trend at a larger upwelling scale. The comparison of the PP at geographical locations between the LGMstd and PD simulations show little change between 1000 and 3000 m depth (Figure 10a), whereas the comparison of the zonally cumulative PP decreases significantly at all latitudes and positions on the slope, but for two narrow

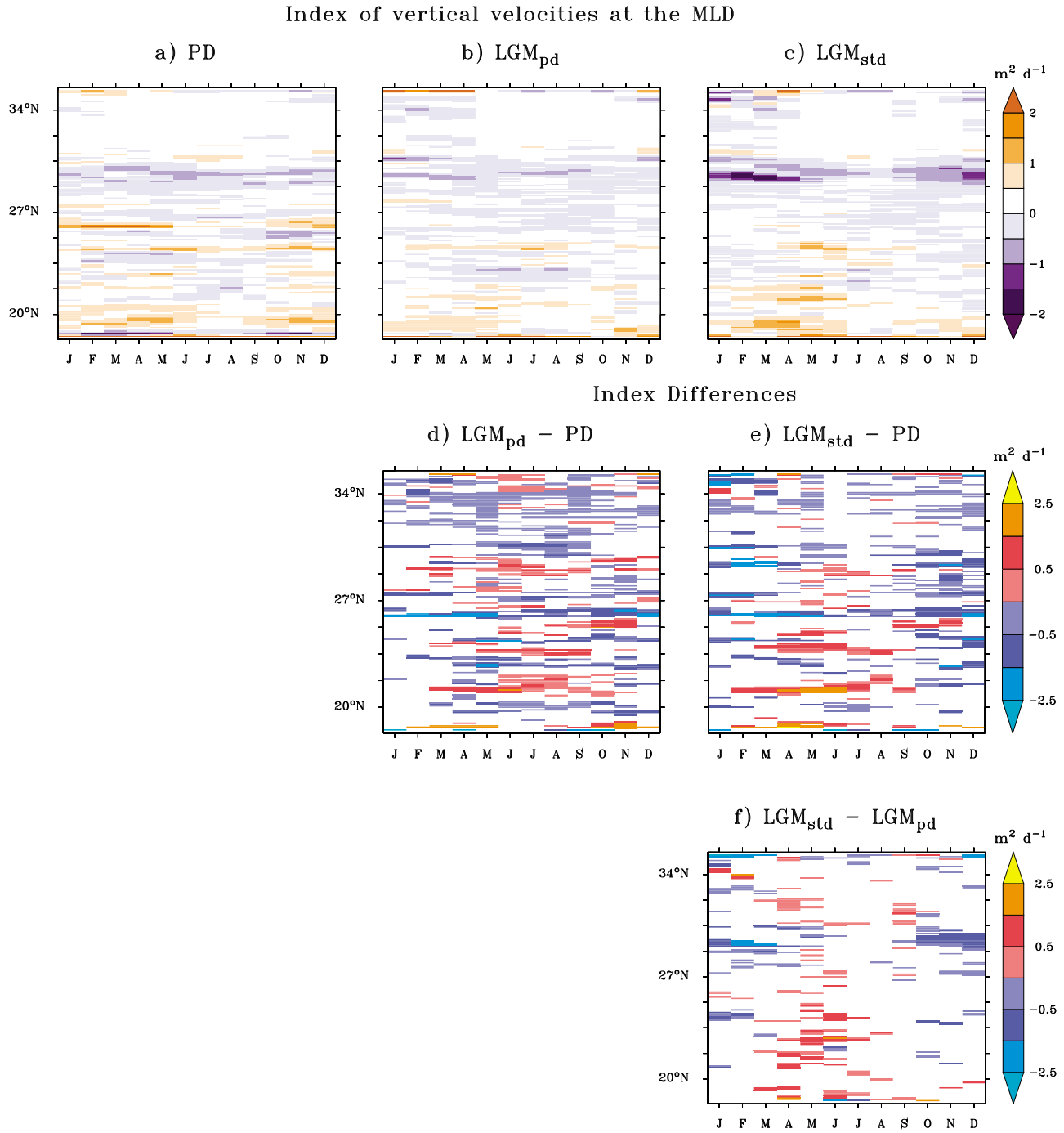

Figure 8. Index of vertical velocities (positive upward) at MLD ($m^2\ d^{-1}$) averaged from the coast to the isodepth 3000 m. A 4-point averaging filter has been applied prior to the zonal averaging and computation of statistical significance. (a) PD, (b) LGMpd, (c) LGMstd, (d) LGMpd-PD, (e) LGMstd-PD, and (f) LGMstd-LGMpd. In Figures 8d–8f, white areas indicate results that are statistically not significant (Student's t test, $\alpha = 0.05$).

bands around ~22°N and ~26°N (Figure 10c). The reason for this discrepancy is the eastward shift of the upwelling center due to the sea level rise from LGM to PD. Because of the topography change, the core sites are not at the same position relative to the maximum production center of the upwelling, i.e., the coastal area. Figures 11a and 11b illustrate the effect of the shoreline shift (due to the sea level change) on the relative position of the longitudinal transects of PP and zonally cumulative PP at both PD and LGM, for the particular example of a transect at 23.3°N. On

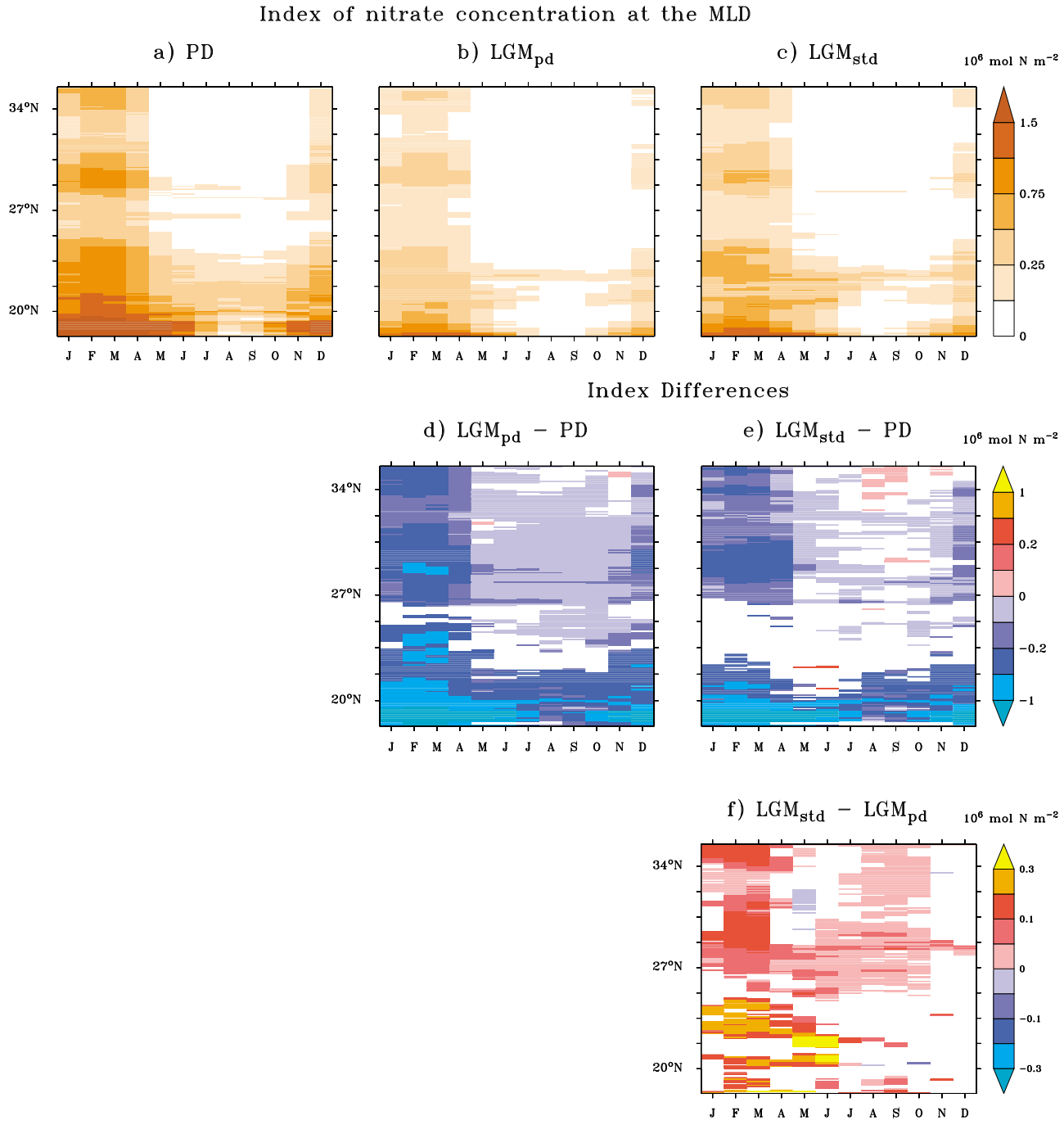

Figure 9. Index of nitrate concentration at MLD (10^6 mol N m^{-2}) averaged from the coast to the isodepth 3000 m. (a) PD, (b) LGMpd, (c) LGMstd, (d) LGMpd-PD, (e) LGMstd-PD, and (f) LGMstd-LGMpd. In Figures 9d–9f, white areas indicate results that are statistically not significant (Student's t test, $\alpha = 0.05$).

Figure 11a, the PP of simulation PD (continuous line) and simulation LGMstd (dashed line) overlap remarkably. The comparison of the PP at geographical locations of these two simulations does not show a significant change at this latitude (see also Figure 10a). However, when reported to the same longitudinal start (continuous line versus dotted line), these two simulations show different cross-shore profiles of PP, indicating clearly that the LGMpd simulation is globally less productive at this latitude. This is even clearer on Figure 11b where the zonally cumulative PP is plotted.

[48] Second, the fact that the data do not match any of the interpretations of the simulation LGMstd suggests that the model is inadequate or that the interpretation of the data is problematic. In particular, it is not possible to explain the apparent increase in PP as indicated by the data of cores north of 22°N. Section 5.2 considers the hypothesis of a

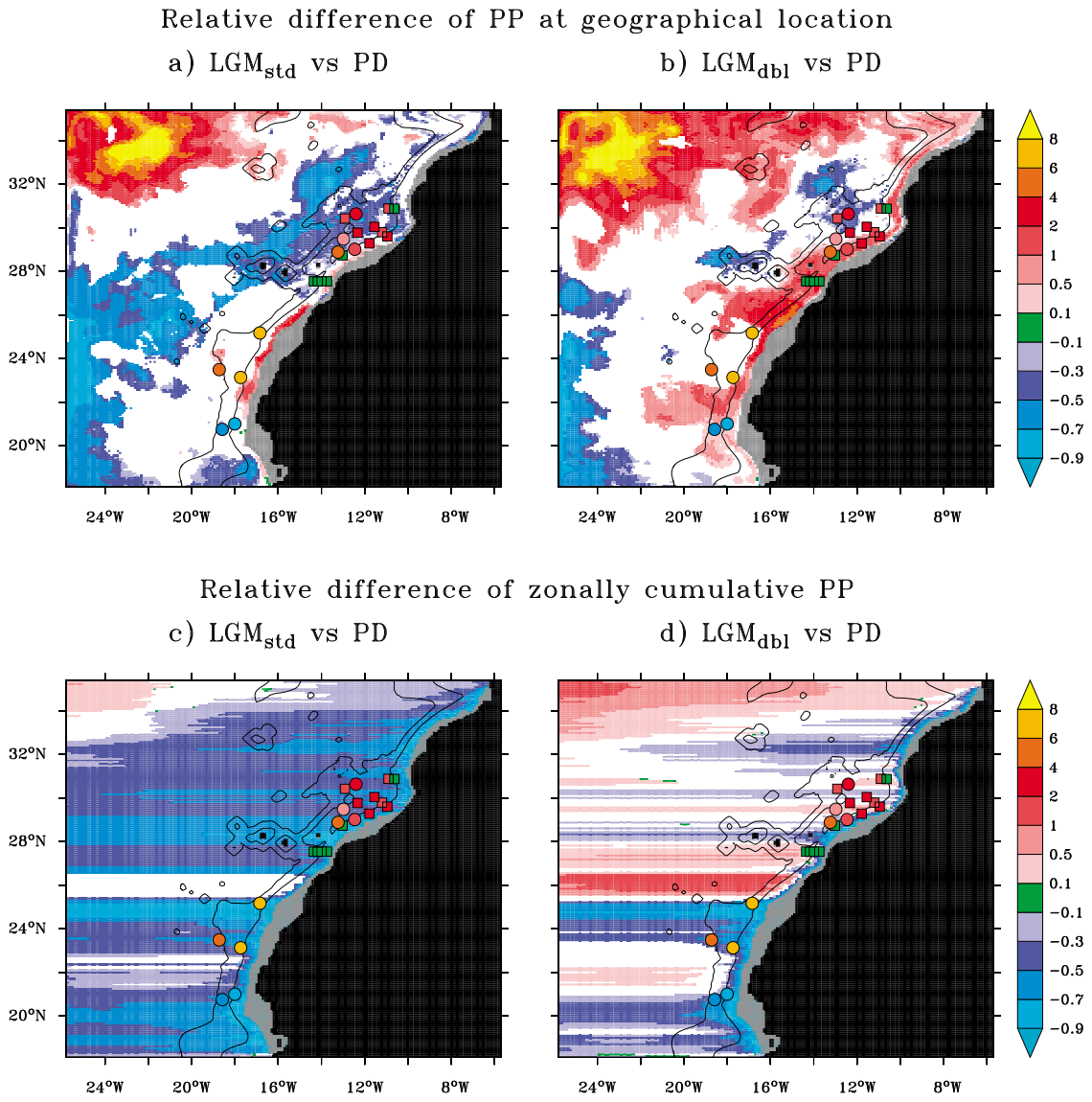

Figure 10. Relative difference of PP between LGM and PD simulations (LGM/PD-1): Vertically integrated PP at geographical location comparing (a) LGMstd versus PD and (b) LGMdbl versus PD. Zonally cumulative PP between any location and the coast comparing (c) LGMstd versus PD and (d) LGMdbl versus PD. Circles and squares are data as presented in Figure 1.

stronger wind stress during the LGM over the NW African coast.

5.2. Wind Stress Sensitivity Test

[49] An early study of dust accumulation in marine sediments over the eastern subtropical Atlantic and NW Africa concluded that the Harmattan and Trade Wind systems strengthened during the last glacial period, without changes in the latitudinal position of the summer ITCZ [*Sarnthein et al.*, 1981]. The increased wind intensity has also been asserted by further core studies at the latitude of Cape Blanc based on grain-size analysis [e.g., *Martinez et al.*, 1999; *Zhao et al.*, 2000] or terrestrial biomarkers records [*Sicre et al.*, 2001]. This is in stark contrast to the wind stress field used in simulation LGMstd, which showed hardly any change in this region. Simulation LGMdbl has been designed to test the impact of increased local wind intensity. The wind stress has been doubled in a restricted area localized along the coast of our study area (see Appendix A for a description). The perturbation is applied only locally in order to evaluate a local answer and not a change in the basin-scale circulation.

[50] Doubling the wind strength over the coastal area, as introduced in simulation LGMdbl, led to an overall increase of the PP. This is true for both approaches of comparing the PP at geographical location or zonally (Figures 10b and 10d). Despite this general increase in PP, the two approaches used to evaluate the changes in local or zonal PP can still give different LGM to PD trends, as previously demonstrated, or even opposite trends. This is illustrated on Figures 11c and 11d, where we plotted the transect of PP and zonally

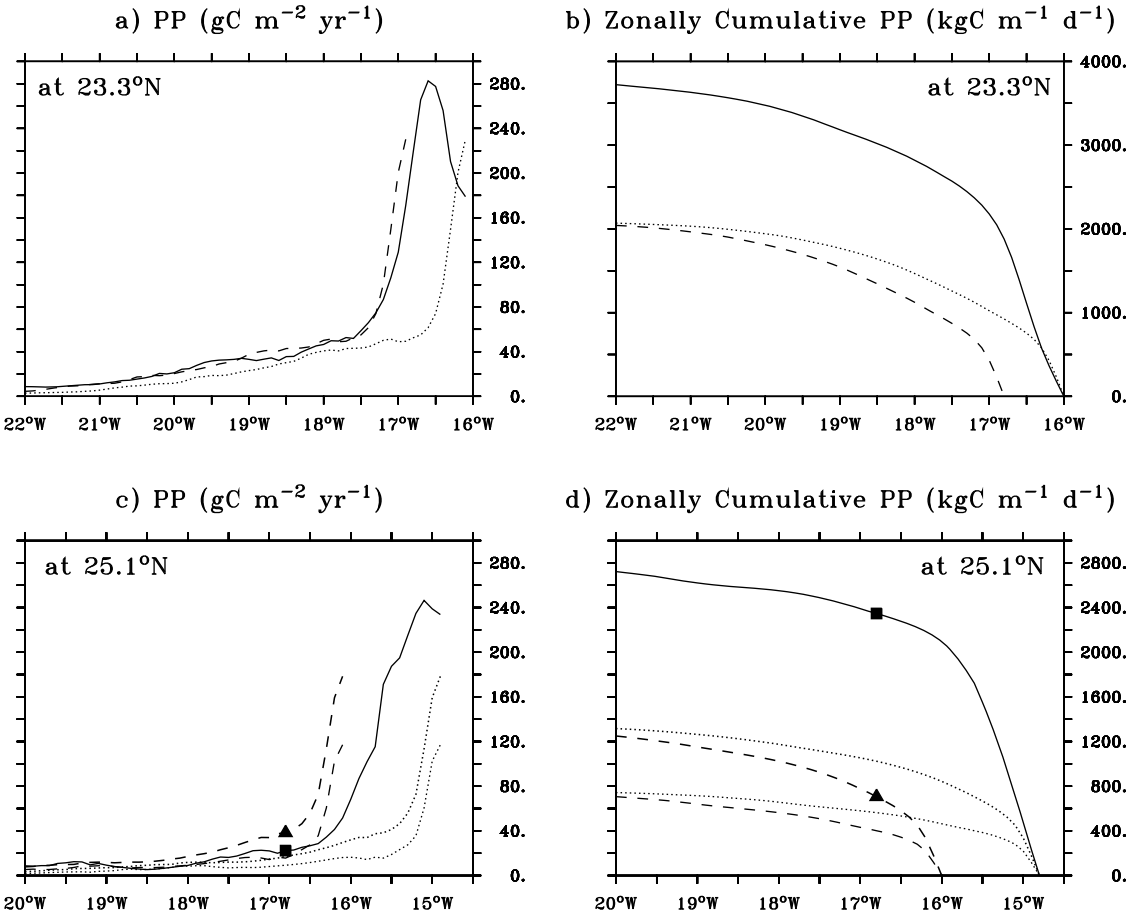

Figure 11. Longitudinal transects of modeled PP and zonally cumulative PP at (a and b) 23.3°N and (c and d) 25.1°N. Simulation PD (continuous line), LGMpd (dashed thin line), LGMdbl (dashed bold line). Dotted lines (thin and bold) are identical to dashed lines (thin and bold, respectively), but shifted eastward in order to start at the same longitude than the PD simulation, for comparison purposes only. The square and triangle marks in Figures 11c and 11d indicate the longitude of core GIK12392-1 (at 16.84°W–25.17°N, see Table 1) for simulations PD and LGMdbl, respectively.

cumulative PP at 25.1°N, for the simulations PD (continuous line), simulation LGMstd (dashed line) and LGMdbl (bold dashed line). We also indicate the location of core GIK12392–1 (at 16.8°W, 2575 m depth), for both simulations PD (square symbol) and LGMdbl (triangle symbol). At this particular location, the zonally cumulative PP at LGMdbl (triangle on Figure 11d) is significantly lower than the zonally cumulative PP at PD (square on Figure 11d). We could therefore conclude that, at this particular transect, the LGMdbl simulation is globally less productive. However, because of the sea level change and the associated eastward shift of the coastline and upwelling system, the local PP at LGMdbl (triangle on Figure 11c) appears to be significantly higher than the local PP at PD (square on Figure 11c), which is at the opposite of the interpretation given by the zonally cumulative PP.

[51] Nevertheless, it is now possible to find a scenario to match the model outputs with the sedimentary data. To do so, we propose to distinguish between the core sites off Cape Blanc, where the sedimentary signal may record the zonal production, from the rest of the area, where the sedimentary cores may record the local PP. In the two sites off Cape Blanc, around 21°N, the presence of the slope depocenter [*Fütterer*, 1983] points to the processes of remobilization and accumulation of the sediments. Therefore we compare the data to the trend of the zonal production in the model result (Figure 10b). They agree about the decrease in PP from PD to LGM. The other sedimentary cores in the north are not known to face a slope depocenter [*Fütterer*, 1983]. We compare therefore the data to the local production of model results (Figure 10d). The data indicate an increase of the PP while the model simulates either an increase or no significant change. Assuming a different meaning of the sedimentary record (local in the north, and zonal off Cape Blanc), the scenario of a doubling in wind stress over the NW African upwelling leads to an agreement between data and model results.

5.3. Subsurface Nutrients Versus Local Conditions

[52] Figure 5f shows that the simulation LGMstd is significantly more productive than simulation LGMpd close to

the coast and at many locations over the continental slope. Since the bathymetry is identical for both LGM simulations, this local PP difference was not due to any sea level change effect. It may therefore reflect the changes in upward flux of nutrients, which is itself a result of variations of both the vertical velocities, i.e., the upward flux of subsurface waters, and the nutrient content of these upwelling subsurface waters.

[53] The vertical velocities are driven by the local surface wind stress and the process of Ekman pumping. In this sense it belongs to local conditions, even if the wind field has a large deformation radius and can be seen as a synoptic feature. On the other hand, the subsurface nutrient concentration is not controlled by regional biogeochemical processes. Even if some effects of transient nutrient trapping may have existed in the model, the remineralization of organic matter at the regional scale played a minor role in renewing the nutrient content of subsurface waters. The latter was mainly controlled by the conditions during the formation of central water by ventilating the thermocline and the remineralization of organic matter during the circulation. The subsurface nutrients were therefore formed outside of our study area, i.e., preformed, and respond to basin scale conditions.

[54] The results of Figure 8f showed that the use of LGM wind stress conditions for simulation LGMstd instead of the PD wind stress for simulation LGMpd did not significantly modify the vertical velocities at the MLD. Therefore, we conclude that the wind stress variations issued from the CCSM3 wind stress anomaly played a minor role in driving the PP variations if we consider the local process of Ekman pumping. This result is in agreement with the fact that the CCSM3 wind stress anomaly did not significantly modify the PD wind stress in the coastal area of NW Africa. The sensitivity test introduced in section 5.2 identified the role of an increased wind stress on the upwelling PP.

[55] The MLD of simulation LGMstd was shallower than for simulation LGMpd (Figure 7f). This was a response to the local wind stress conditions. Despite this shallower MLD, the nutrient concentration at the MLD was higher for LGMstd than for LGMpd (Figure 9f). The CCSM3 wind stress anomaly was the only change in forcing conditions between the two LGM simulations performed with the UVic model. The CCSM3 wind stress anomaly had therefore an influence on the PP of the NW African coastal upwelling by inducing the formation of subsurface waters with a higher nutrient content.

[56] In winter, the PP of this upwelling area was the result of the deepening of the MLD rather than of the upwelling of subsurface waters. The deepening of the winter MLD was less intense for LGMstd than for LGMpd (Figure 7f), so that despite higher subsurface nutrient concentrations for LGMstd (Figure 9f), the availability of nutrients for the mixed layer was similar for both LGM simulations and did not induce any significant change in winter PP (not shown). The CCSM3 wind stress anomaly introduced in simulation LGMstd compared to LGMpd had no net impact on the winter PP, because local (i.e., shallower MLD driven by local wind stress) and global (higher preformed subsurface nutrient concentration) canceled each other. The decrease of winter PP for LGMstd compared to PD was already present in simulation LGMpd. The winter PP decrease between PD and LGM simulations was therefore due to the decrease in preformed subsurface nutrient content at the basin scale (Figures 9d and 9e) and the LGM boundary conditions, not the local CCSM3 wind stress anomaly.

[57] In summer, the PP of this upwelling area was driven by the upward flux of subsurface nutrients. Figure 8f shows that the CCSM3 wind stress anomaly did not induce a significant change in vertical velocities at the MLD between the two LGM simulations. Figure 9f shows that north of ~26°N, the nutrient concentration at MLD was higher in summer for LGMstd than for LGMpd, while the MLD itself did not significantly change (Figure 7f). As a consequence, the summer PP was higher for LGMstd than for LGMpd (not shown). South of 26°N, the combination of statistically non-significant changes in vertical velocities and nutrient concentration at MLD still induced a significant increase of PP. We consider that it was due to the combination of nonlinear processes. We conclude that, in summer, the CCSM3 wind stress anomaly introduced in simulation LGMstd compared to LGMpd, had a net positive impact on the PP, because of higher preformed subsurface nutrient concentration, while the local factors stay unchanged, i.e., identical MLD (Figure 7f) and vertical velocities (Figure 8f) driven by local wind stress.

[58] Despite this increase in subsurface nutrient concentration compared to LGMpd, the LGMstd PP remained lower than for PD, except for some narrow bands. The lower summer PP observed in both LGM simulations was the result of higher vertical velocities and lower or not modified subsurface nutrient concentrations. The local favorable conditions, i.e., higher upwelling intensity, did not compensate for the global non-favorable changes, i.e., lower preformed nutrient concentration. It is also worth noting that the increase in summer upwelling intensity was due to the sea level and topography change, not to the variations in surface wind stress (see section 4.4.3). Therefore, both for winter and summer conditions, the changes in subsurface nutrient concentration predominantly drive the upwelling PP.

6. Conclusion

[59] Based on regional coupled simulations, we investigated the processes driving the variations of PP in the NW African coastal upwelling area during glacial times and its record in sediments, with a particular interest in the effect of sea level change. We conclude that annual-mean SST changes along the coast reflected the general trend of the North Atlantic cooling at the LGM, but that they may not be related to variations in upwelling intensity. We used two approaches to compare the PP variations between glacial and interglacial time. First, we compared the PP at geographical locations, assuming a direct link between the surface signal and the sedimentary record below. Second, we calculated the zonal integration of the PP between the coast and any location, considering that advection and sediment transport processes had the effect of summing up the signal produced mostly over the continental shelf. The zonally cumulative PP of our standard LGM simulation (LGMstd) showed a decrease compared to the present day,

at all latitudes of our study area. This could be caused by the nutrient depletion of glacial subsurface waters and/or the shift of the upwelling center toward the continental slope because of the lower sea level. In contrast, the comparison of the PP at geographical locations between LGMstd and PD over the continental slope did not show significant changes. This is explained by the fact that the area of maximum production during the LGM is now displaced over the continental slope, where the PD upwelling was already in a less eutrophic stage. Therefore, variations of PP from LGM to PD for a core site can show variations or not, depending on whether it is a record of the local production or of the zonally cumulative production. This decoupling between geographical PP and zonal PP was attributed to the eastward shift of the coastline due to the sea level rise from the LGM to the PD. Before interpreting a sedimentary signal, it is therefore important to make sure whether it is representative of the zonally cumulative production, or of the local production. In a sensitivity experiment, the doubling of wind stress localized over NW Africa has shown the same decoupling between PP at geographical location and zonal PP.

[60] With this work, we have attempted to evaluate the relative importance of sea level, wind strength and subsurface nutrient concentration in the variations of glacial PP of the coastal upwelling. Based on a global simulation of LGM conditions, we used boundary and initial conditions showing a subsurface nutrient depletion of ~32%. First, this nutrient depletion seemed to be the main reason to explain the decrease of the zonal PP observed in our simulations. Second, the sea level change induced a change in the upwelling intensity that increased the PP of the upwelling. This increase in PP only partly compensated the decrease induced by the reduced subsurface nutrient concentration. Third, the LGM wind field introduced in our LGMstd simulation (the CCSM3 wind stress anomaly added to the NCEP/NCAR present-day wind field) had little influence at the local scale on the LGM PP. However, a sensitivity experiment showed that a doubling of the wind stress localized over the NW African coast had a significant impact on the PP, leading to an increased PP.

[61] From this study, it appears clearly that the interpretation of a sedimentary signal as a record of local conditions cannot be extrapolated to an entire upwelling area; there is a decoupling between the local and regional scales. Further advances regarding the effect of changes in sea level, subsurface nutrient concentration and wind strength on glacial PP variations will depend on our understanding of sediment origin, transport processes and sediment distribution on the continental slope. These should be included in numerical models.

Appendix A

[62] The wind stress of simulation LGMdbl has been modified in order to double the wind stress over a restricted area of the NW African coast. We consider two arbitrary reference points A (18.5°N, 19.0°W) and B (33.0°N, 9°W), located along the NW African coast. For any point P of the model domain, we calculate the sum L of distances AP and BP. For any point of the domain where L is less than a critical distance L_{cr} = 1200 km, we apply a scale factor W_{scale} to the wind stress as follows:

$$W_{scale} = 1 + \frac{1}{2}\left[1 + \sin\left(\pi\left(L/L_{crit} + \frac{1}{2}\right)\right)\right] \quad \text{if } L < L_{crit}$$

$$W_{scale} = 1 \quad \text{if } L \geq L_{crit}$$

[63] **Acknowledgment.** This work was funded through the DFG Research Center/Excellence Cluster "The Ocean in the Earth System."

References

Armstrong, E. M., and J. Vazquez-Cuervo (2001), A new global satellite-based sea surface temperature climatology, *Geophys. Res. Lett.*, *28*(22), 4199–4202, doi:10.1029/2001GL013316.

Bard, E., B. Hamelin, M. Arnold, L. Montaggioni, G. Cabioch, G. Faure, and F. Rougerie (1996), Deglacial sea-level record from Tahiti corals and the timing of global meltwater discharge, *Nature*, *382*(6588), 241–244, doi:10.1038/382241a0.

Berelson, W. M. (2002), Particle settling rates increase with depth in the ocean, *Deep Sea Res., Part II*, *49*(1–3), 237–251, doi:10.1016/S0967-0645(01)00102-3.

Berger, A. (1978), Long-term variations of caloric insolation resulting from the Earth's orbital elements, *Quat. Res.*, *9*(2), 139–167, doi:10.1016/0033-5894(78)90064-9.

Blayo, E., and L. Debreu (1999), Adaptive mesh refinement for finite-difference ocean models: First experiments, *J. Phys. Oceanogr.*, *29*(6), 1239–1250, doi:10.1175/1520-0485(1999)029<1239:AMRFFD>2.0.CO;2.

Debreu, L. (2000), Adaptive mesh refinement and zoom techniques: Application to ocean models (in French), Univ. Joseph Fourier de Grenoble 1, Grenoble, France.

Debreu, L., C. Vouland, and E. Blayo (2008), AGRIF: Adaptive grid refinement in Fortran, *Comput. Geosci.*, *34*(1), 8–13, doi:10.1016/j.cageo.2007.01.009.

Diester-Haas, L. (1983), Differentiation of high oceanic fertility in marine sediments caused by coastal upwelling and/or river discharge off Northwest Africa during the late Quaternary, in *Coastal Upwelling: Its Sedimentary Record, Part B: Sedimentary Records of Ancient Coastal Upwelling*, edited by J. Thiede and E. Suess, pp. 399–419, Plenum, New York.

Eberwein, A., and A. Mackensen (2008), Last Glacial Maximum paleoproductivity and water masses off NW-Africa: Evidence from benthic foraminifera and stable isotopes, *Mar. Micropaleontol.*, *67*(1–2), 87–103, doi:10.1016/j.marmicro.2007.08.008.

Fischer, G., B. Donner, V. Ratmeyer, R. Davenport, and G. Wefer (1996), Distinct year-to-year particle flux variations off Cape Blanc during 1988–1991: Relation to δ^{18}O-deduced sea-surface temperatures and trade winds, *J. Mar. Res.*, *54*(1), 73–98, doi:10.1357/0022240963213484.

François, R., M. Frank, M. M. R. van der Loeff, and M. P. Bacon (2004), Th-230 normalization: An essential tool for interpreting sedimentary fluxes during the late Quaternary, *Paleoceanography*, *19*, PA1018, doi:10.1029/2003PA000939.

Freudenthal, T., and H. Kuhlmann (2001), Age model and TOC of sediment core GeoB4228-3, http://doi.pangaea.de/10.1594/PANGAEA.57857, PANGAEA, Germany.

Freudenthal, T., T. Wagner, F. Wenzhöfer, M. Zabel, and G. Wefer (2001), Early diagenesis of organic matter from sediments of the eastern subtropical Atlantic: Evidence from stable nitrogen and carbon isotopes, *Geochim. Cosmochim. Acta*, *65*(11), 1795–1808, doi:10.1016/S0016-7037(01)00554-3.

Freudenthal, T., H. Kuhlmann, and H. Meggers (2001a), Age model, stable isotope record, CaCO3 and TOC of sediment core GeoB4216-1, http://doi.pangaea.de/10.1594/PANGAEA.57856, PANGAEA, Germany.

Freudenthal, T., H. Kuhlmann, and H. Meggers (2001b), Age model, stable isotope record, CaCO3 and TOC of sediment core GeoB4223-2, http://doi.pangaea.de/10.1594/PANGAEA.57858, PANGAEA, Germany.

Freudenthal, T., H. Kuhlmann, and H. Meggers (2001c), Age model, stable isotope record, CaCO3 and TOC of sediment core GeoB4240-2, http://doi.pangaea.de/10.1594/PANGAEA.57859, PANGAEA, Germany.

Freudenthal, T., H. Meggers, J. Henderiks, H. Kuhlmann, A. Moreno, and G. Wefer (2002), Upwelling intensity and filament activity off Morocco during the last 250,000 years, *Deep Sea Res., Part II*, *49*(17), 3655–3674, doi:10.1016/S0967-0645(02)00101-7.

Fütterer, D. (1983), The modern upwelling record off Northwest Africa, in *Coastal Upwelling: Its Sedimentary Record, Part B: Sedimentary Records of Ancient Coastal Upwelling*, edited by J. Thiede and E. Suess, pp. 105–121, Plenum, New York.

Gabric, A. J., L. Garcia, L. V. Camp, L. Nykjaer, W. Eifler, and W. Schrimpf (1993), Offshore export of shelf production in the Cape Blanc (Mauritania) giant filament as derived from coastal zone color scanner imagery, *J. Geophys. Res.*, *98*(C3), 4697–4712, doi:10.1029/92JC01714.

Garcia, H., R. Locarnini, T. Boyer, and J. Antonov (2006), *World Ocean Atlas 2005*, vol. 4, *Nutrients (Phosphate, Nitrate, Silicate)*, *NOAA Atlas NESDIS 64*, edited by S. Levitus, U.S. Govt. Print. Off., Washington, D. C.

Giraud, X. (2006), Modelling an alkenone-like proxy record in the NW African upwelling, *Biogeosciences*, *3*(3), 251–269, doi:10.5194/bg-3-251-2006.

Giraud, X., P. Bertrand, V. Garçon, and I. Dadou (2000), Modeling delta N-15 evolution: First palaeoceanographic applications in a coastal upwelling system, *J. Mar. Res.*, *58*(4), 609–630, doi:10.1357/002224000321511043.

Giraud, X., P. Bertrand, V. Garçon, and I. Dadou (2003), Interpretation of the nitrogen isotopic signal variations in the Mauritanian upwelling with a 2D physical-biogeochemical model, *Global Biogeochem. Cycles*, *17*(2), 1059, doi:10.1029/2002GB001951.

Hartmann, M., P. J. Müller, E. Suess, and C. H. Weijden (1976), Chemistry of Late Quaternary sediments and their interstitial waters of sediment cores from the North-West African continental margin, http://doi.pangaea.de/10.1594/PANGAEA.548430, PANGAEA, Germany.

Kageyama, M., A. Paul, D. M. Roche, and C. J. Van Meerbeeck (2010), Modelling glacial climatic millennial-scale variability related to changes in the Atlantic meridional overturning circulation: a review, *Quat. Sci. Rev.*, *29*, 2931–2956, doi:10.1016/j.quascirev.2010.05.029.

Kalnay, E., et al. (1996), The NCEP/NCAR 40-year reanalysis project, *Bull. Am. Meteorol. Soc.*, *77*(3), 437–471, doi:10.1175/1520-0477(1996)077<0437:TNYRP>2.0.CO;2.

Kara, A. B., P. A. Rochford, and H. E. Hurlburt (2000), An optimal definition for ocean mixed layer depth, *J. Geophys. Res.*, *105*(C7), 16,803–16,821, doi:10.1029/2000JC900072.

Klaas, C., and D. E. Archer (2002), Association of sinking organic matter with various types of mineral ballast in the deep sea: Implications for the rain ratio, *Global Biogeochem. Cycles*, *16*(4), 1116, doi:10.1029/2001GB001765.

Kriest, I. (2002), Different parameterizations of marine snow in a 1D-model and their influence on representation of marine snow, nitrogen budget and sedimentation, *Deep Sea Res., Part I*, *49*(12), 2133–2162, doi:10.1016/S0967-0637(02)00127-9.

Kriest, I., and G. T. Evans (1999), Representing phytoplankton aggregates in biogeochemical models, *Deep Sea Res., Part I*, *46*(11), 1841–1859, doi:10.1016/S0967-0637(99)00032-1.

Large, W., J. McWilliams, and S. Doney (1994), Oceanic vertical mixing: A review and a model with a nonlocal boundary layer parameterization, *Rev. Geophys.*, *32*(4), 363–403, doi:10.1029/94RG01872.

Martinez, P., P. Bertrand, G. B. Shimmield, K. Cochrane, F. J. Jorissen, J. Foster, and M. Dignan (1999), Upwelling intensity and ocean productivity changes off Cape Blanc (northwest Africa) during the last 70,000 years: Geochemical and micropalaeontological evidence, *Mar. Geol.*, *158*(1–4), 57–74, doi:10.1016/S0025-3227(98)00161-3.

Meissner, K. J., A. J. Weaver, H. D. Matthews, and P. M. Cox (2003), The role of land surface dynamics in glacial inception: A study with the UVic Earth System Model, *Clim. Dyn.*, *21*(7–8), 515–537, doi:10.1007/s00382-003-0352-2.

Mollenhauer, G., M. Inthorn, T. Vogt, M. Zabel, J. S. Sinninghe Damsté, and T. I. Eglinton (2007), Aging of marine organic matter during cross-shelf lateral transport in the Benguela upwelling system revealed by compound-specific radiocarbon dating, *Geochem. Geophys. Geosyst.*, *8*, Q09004, doi:10.1029/2007GC001603.

Morel, A. (2000), Process studies in eutrophic, mesotrophic and oligotrophic oceanic regimes within the tropical northeast Atlantic, in *The Changing Ocean Carbon Cycle*, edited by R. B. Hanson, H. W. Ducklow, and J. G. Field, pp. 338–374, Cambridge Univ. Press, New York.

National Geophysical Data Center (1988), Digital relief of the surface of the Earth. Boulder, *Announce. 88-MGG-02*, NOAA, Boulder, Colo.

Oschlies, A., and V. Garçon (1999), An eddy-permitting coupled physical-biological model of the North Atlantic: 1. Sensitivity to advection numerics and mixed layer physics, *Global Biogeochem. Cycles*, *13*(1), 135–160, doi:10.1029/98GB02811.

Otto-Bliesner, B. L., C. D. Hewitt, T. M. Marchitto, E. Brady, A. Abe-Ouchi, M. Crucifix, S. Murakami, and S. L. Weber (2007), Last Glacial Maximum ocean thermohaline circulation: PMIP2 model intercomparisons and data constraints, *Geophys. Res. Lett.*, *34*, L12706, doi:10.1029/2007GL029475.

Pacanowski, R. C. (1995), *MOM 2 Documentation User's Guide and Reference Manual*, *Version 1.0, GFDL Tech. Rep. 3*, Geophys. Fluid Dyn. Lab., Princeton, N. J.

Parkin, D. W. (1974), Trade-winds during the glacial cycles, *Proc. R. Soc. London, Ser. A*, *337*, 73–100, doi:10.1098/rspa.1974.0039.

Parkin, D. W., and N. J. Shackleton (1973), Trade wind and temperature correlations down a deep-sea core off the Saharan coast, *Nature*, *245*(5426), 455–457, doi:10.1038/245455a0.

Peltier, W. R. (2004), Global glacial isostasy and the surface of the Ice-Age Earth: The ICE-5G (VM2) model and GRACE, *Annu. Rev. Earth Planet. Sci.*, *32*, 111–149, doi:10.1146/annurev.earth.32.082503.144359.

Penven, P., L. Debreu, P. Marchesiello, and J. C. McWilliams (2006), Evaluation and application of the ROMS 1-way embedding procedure to the central California upwelling system, *Ocean Modell.*, *12*(1–2), 157–187, doi:10.1016/j.ocemod.2005.05.002.

Rühlemann, C., P. J. Müller, and R. Schneider (1999), Organic carbon and carbonate as paleoproductivity proxies: Examples from high and low productivity areas of the tropical Atlantic, in *Use of Proxies in Paleoceanography: Examples from the South Atlantic*, edited by G. Fischer and G. Wefer, pp. 315–344, Springer, New York.

Sarnthein, M., G. Tetzlaff, B. Koopmann, K. Wolter, and U. Pflaumann (1981), Glacial and inter-glacial wind regimes over the eastern sub-tropical Atlantic and northwest Africa, *Nature*, *293*(5829), 193–196, doi:10.1038/293193a0.

Schmittner, A., A. Oschlies, H. D. Matthews, and E. D. Galbraith (2008), Future changes in climate, ocean circulation, ecosystems, and biogeochemical cycling simulated for a business-as-usual CO_2 emission scenario until year 4000 AD, *Global Biogeochem. Cycles*, *22*, GB1013, doi:10.1029/2007GB002953.

Shchepetkin, A. F., and J. C. McWilliams (2003), A method for computing horizontal pressure-gradient force in an oceanic model with a nonaligned vertical coordinate, *J. Geophys. Res.*, *108*(C3), 3090, doi:10.1029/2001JC001047.

Shchepetkin, A. F., and J. C. McWilliams (2005), The regional oceanic modeling system (ROMS): A split-explicit, free-surface, topography-following-coordinate oceanic model, *Ocean Modell.*, *9*(4), 347–404, doi:10.1016/j.ocemod.2004.08.002.

Sicre, M. A., Y. Ternois, M. Paterne, A. Boireau, L. Beaufort, P. Martinez, and P. Bertrand (2000), Biomarker stratigraphic records over the last 150 kyears off the NW African coast at 25°N, *Org. Geochem.*, *31*(6), 577–588, doi:10.1016/S0146-6380(00)00021-8.

Sicre, M. A., Y. Ternois, M. Paterne, P. Martinez, and P. Bertrand (2001), Climatic changes in the upwelling region off Cap Blanc, NW Africa, over the last 70 kyear: A multi-biomarker approach, *Org. Geochem.*, *32*(8), 981–990, doi:10.1016/S0146-6380(01)00061-4.

Sigman, D. M., S. J. Lehman, and D. W. Oppo (2003), Evaluating mechanisms of nutrient depletion and ^{13}C enrichment in the intermediate-depth Atlantic during the last ice age, *Paleoceanography*, *18*(3), 1072, doi:10.1029/2002PA000818.

Speth, P., and H. Detlefsen (1982), Meteorological influences on upwelling off Northwest Africa, *Rapp. P. V. Reun. Cons. Int. Explor. Mer*, *180*, 29–34.

Tiedemann, R. (1991), Accumulation rates calculated for Site 108-658, http://doi.pangaea.de/10.1594/PANGAEA.68589, PANGAEA, Germany.

Weaver, A., et al. (2001), The UVic Earth System Climate Model: Model description, climatology, and applications to past, present and future climates, *Atmos. Ocean*, *39*(4), 361–428.

Zhao, M. X., G. Eglinton, S. K. Haslett, R. W. Jordan, M. Sarnthein, and Z. H. Zhang (2000), Marine and terrestrial biomarker records for the last 35,000 years at ODP site 658C off NW Africa, *Org. Geochem.*, *31*(9), 919–930, doi:10.1016/S0146-6380(00)00027-9.

X. Giraud, CEREGE, Aix-Marseille Université, Collège de France, IRD, Europôle de l'Arbois, CNRS, BP80, F-13545 Aix-en-Provence, France. (giraud@cerege.fr)

A. Paul, MARUM – Center for Marine Environmental Sciences and Faculty of Geosciences, University of Bremen, PO Box 33 04-40, D-28334 Bremen, Germany.